Microchimica Acta (2020) 187:671
https://doi.org/10.1007/s00604-020-04635-7

ORIGINAL PAPER

# A 433-MHz surface acoustic wave sensor with Ni-$TiO_2$-poly(L-lysine) composite film for dopamine determination

Jingyi Han[1] · Mingji Li[1] · Hongji Li[2] · Huayi Li[1] · Cuiping Li[1] · Honglang Li[3] · Lirong Qian[1] · Baohe Yang[1]

Received: 28 July 2020 / Accepted: 6 November 2020


## Abstract

A ternary hybrid material composed of Ni nanoparticles (NPs), $TiO_2$ NPs, and poly(L-lysine) (Ply) was used as a sensing material. It was electrodeposited in situ onto a commercial 433-MHz surface acoustic wave (SAW) resonator to construct a Ni-$TiO_2$-Ply/SAW sensor. The Ni-$TiO_2$-Ply sensing layer fully covered the resonant cavity of the SAW resonator. As the sensing layer completely covers the interdigital transducer and piezoelectric substrate, the sensing area is significantly increased, and the resonator is protected from damage or contamination. To detect the level of dopamine (DA) in serum, the fabrication of the Ni-$TiO_2$-Ply sensing layer, distributions of various components in the sensing layer, and responses of the SAW biosensor to DA were investigated in detail. In addition, an electric field-assisted liquid-phase oxidation technique was developed for loading analytes onto the SAW sensors. After optimizing the pH value and L-lysine content of the sensing layer electrolyte and the pH value of the DA solution, the SAW biosensor responded to DA with a linear concentration range of 1 to 1000 nM, sensitivity of 5.77 MHz $nM^{-1}$ $cm^{-2}$, and limit of detection of 0.067 nM. Moreover, the sensor exhibited good selectivity, reproducibility, and stability at ambient temperature.

**Keywords** Poly(L-lysine) · Nickel · $TiO_2$ · Surface acoustic wave · Biosensor · Dopamine determination

## Introduction

Dopamine (DA, 3,4-dihydroxyphenethylamine) is a neurochemical whose signals are among the most important indicators of brain disorders and diseases [1, 2]. For instance, degradation of the brain DA neurons causes deficient levels of DA, indicating schizophrenia and Parkinson's disease [3, 4]. The DA level in the brain extracellular fluid is generally within the range of 1 to 50 nM [5]. According to reports in the literature, human serum contains DA at widely changing levels of concentration [6, 7]. For the assessment of human ideology in clinical medicine and special environments such as battlefields and harsh climates, DA level determination can provide important reference values.

A number of analysis methods have been developed for DA detection, including high-performance liquid chromatography (HPLC), liquid chromatography-mass spectrometry (LC-MS), fluorescence analysis (FLA), immunoassay, chemiluminescence (CL), electrochemiluminescence (ECL), and electrochemical (EC) methods [8]. Of these, HPLC and LC-MS require cumbersome sample pretreatment processes, and immunoassaying, FLA, and ECL have high test environment requirements, and the EC method is yet to be developed for practical application. Recently, the surface acoustic wave (SAW) technique has been applied to chemical sensors because of its high sensitivity, high stability, low power consumption, low cost, and wireless control capabilities [9, 10]. The SAW sensors that detect DA levels in human sera may enable the

✉ Mingji Li
limingji@163.com

✉ Hongji Li
hongjili@yeah.net

✉ Honglang Li
lhl@cannano.cn

[1] Tianjin Key Laboratory of Film Electronic and Communication Devices, Engineering Research Center of Optoelectronic Devices & Communication Technology (Ministry of Education), School of Electrical and Electronic Engineering, Tianjin University of Technology, Tianjin 300384, People's Republic of China

[2] Tianjin Key Laboratory of Organic Solar Cells and Photochemical Conversion, Tianjin Key Laboratory of Drug Targeting and Bioimaging, School of Chemistry and Chemical Engineering, Tianjin University of Technology, Tianjin 300384, People's Republic of China

[3] National Center for Nanoscience and Technology (NCNST), Beijing 100190, People's Republic of China

Published online: 23 November 2020

development of wireless sensor network nodes because SAW resonators are used in wireless communication devices.

In human body fluids, the levels of biomarkers are mostly reflected by their concentrations in solution [11]. The SAW delay lines and two-port resonators are assembled into liquid-phase SAW biosensors direct or in combination with microfluidic channels [12–14]. In general, the sensing material of a SAW sensor is attached to the delay zone between the input and output interdigital transducers (IDTs), i.e., the nonexcitation zone [13, 15, 16]. The size of the SAW resonator decreases significantly with increasing frequency. For example, as the frequency of the SAW device increases from 100 MHz to 1 GHz, its size decreases from 8 to 1 mm [10]. Typically, to expand the sensing area, the size of the SAW sensor is increased, i.e., a low-frequency device is manufactured [16]. Among SAW sensors with the same sensing layers, high-frequency devices are more sensitive than low-frequency devices, mainly because the high-frequency devices have narrow frequency bands [17–19].

In fact, the IDTs of the SAW device can also be used as attachment points for sensing materials. In 2020, the use of all the excitation zones of the delay line (165.2 MHz) to construct the sensing layers was reported [20]. A 433-MHz single-port SAW resonator has the advantages of relatively high frequency, narrow frequency band, and small size [21]. In our previous work, graphene-Ni-L-alanine composite was modified for a 433-MHz SAW resonator to detect $CO_2$ gas, which verified the feasibility of fully covering the resonant cavity with the sensing material and increasing the sensing area [22].

Electrochemical methods have been quantitatively analyzed based on the proportional relationships between the analyte concentration and electrocatalytic signals [23, 24]. The electrocatalytic signal is obtained from only a small part of the analyte that diffuses or is adsorbed on the sensor surface; that is, not all of the molecules of the analyte in the solution are attached to the sensor. It can be seen that the number of biomarkers attaching to the sensor will be proportional to the concentration of biomarkers in the bodily fluid. Based on this, we propose an electric field-assisted liquid-phase oxidation technology to electrically adsorb biomarkers, that is, a SAW sensor serves as an electrochemical working electrode for the electrical attachment of biomarkers to the sensing layer.

Compared with the extensive literature on the electrochemical detection of DA, only a few works have reported SAW sensors for the biomolecule detection [23]. For example, Maouch et al. [25] prepared a polypyrrole molecular imprinting polymer film modified on the 104-MHz SAW delay zone to achieve selective detection of DA, within a limit of detection (LOD) of 10 nM. Fourati et al. [15] constructed a SAW sensor by modifying the cobalt phthalocyanine thin film on the gold-sensing area, with a low LOD of 0.1 nM for DA. These SAW sensors can achieve specific determination of DA: the former utilizes the molecularly imprinted chemical reaction of the sensing membrane to DA, whereas the latter utilizes its complex reaction with the sensing materials. However, these SAW sensors are equipped with microfluidic channels and do not involve detection of DA in real samples. Here, it is understood that the sensing layer must have high selectivity for specific biomarkers.

In the molecular structure of DA, the acid dissociation constant of the catechol hydroxyl group (–OH) is $pK_a \approx 9.0$, and it is usually dispersed in the electrolyte in the form of cations [26, 27]. However, DA exhibits a self-polymerization phenomenon, and Ni and $TiO_2$ nanoparticles (NPs) electrocatalyze the carboxylation process (–OOH), resulting in a negative charge [26, 28]. Poly(L-lysine) (Ply) is a biological cationic polymer that has strong electrostatic interaction with biological anions [29]. In addition, H bonds can be formed between Ply (–C=O) and DA (–OH or $NH_2$). Further, the $TiO_2$ NPs are dispersed with numerous hydroxyl groups (–OH) owing to the residual bonds, and there is coordination adsorption between Ni and Ply. Therefore, the Ni-$TiO_2$-Ply sensing layer has not only hydrophobic properties but also high capacity for selective adsorption of DA.

Herein, we report a biosensor based on SAW resonators for the determination of DA level in serum. The SAW biosensor consists of a Ni-$TiO_2$-Ply sensing layer for selective adsorption of DA, Al electrodes as IDT for detecting and exciting the SAWs, and quartz as the piezoelectric substrate. We effectively demonstrate for the first time a sensing layer/IDT/piezoelectric substrate-SAW device structure to detect DA in serum. In addition, we developed an electric field-assisted liquid-phase oxidation technique to attach biomarkers proportionally to the SAW sensing layer. Finally, we report the performance of the proposed sensitive, reliable, and stable sensor for DA detection.

## Experimental section

### Materials and reagents

$Na_2SO_4$ and $NiSO_4$ were purchased from Tianjin Kewei Co., Ltd. (Tianjin, China). $NaH_2PO_4$, $Na_2HPO_4$, $H_3PO_4$, and L-lysine were purchased from Tianjin Guangfu Fine Chemical Research Institute (Tianjin, China). $TiO_2$ NPs were purchased from Siping Gaosida Nano Material Equipment Co., Ltd. (Siping, China). Human serum specimens were purchased from Beijing Solarbio Science and Technology Co., Ltd. (Beijing, China). DA, glucose, and L-lysine were purchased from Sigma-Aldrich. Ultrapure water (18.25 MΩ cm, 24 °C) was used in all the experimental processes.

### Preparation of Ni-$TiO_2$-Ply/SAW sensor

The basic device of the biosensor was a single-port SAW resonator with a central frequency of 433.92 MHz ± 75 kHz,

which was purchased from Beijing Zhongxun Sifang Science and Technology Co., Ltd. (Beijing, China). The piezoelectric substrate was an ST-cut quartz with dimensions 3.62 × 0.82 × 0.33 mm. In total, 160 pairs of Al fingers (IDTs) with individual widths of 2.1 μm, thicknesses of 130 nm, and periods of 7.3 μm were patterned on the ST-cut quartz piezoelectric substrate using the conventional photolithography method (Fig. S1). The IDTs served as acoustic/electric transducers. When an alternating electric signal was applied to the input end of a group of IDTs on the piezoelectric substrate, a periodic electric field was generated. The inverse piezoelectric effect excited an elastic deformation near the surface of the piezoelectric medium, which induced the vibration of solid particles and caused surface acoustic waves to propagate along the surface of the substrate.

Figure 1a shows the electrodeposition process for modifying the Ni-$TiO_2$-Ply sensing film on the SAW device. First, a mixed suspension of 0.1 M $NaSO_4$, 0.1 M $NiSO_4$, 1 mM L-lysine, and 10 mg $mL^{-1}$ $TiO_2$ NPs was prepared using pH 5 phosphate-buffered saline (PBS) solution (0.1 M). Subsequently, electrochemical deposition of the Ni-$TiO_2$-Ply layer was performed in a two-electrode cell comprising a SAW resonator as the working electrode and a Pt wire (diameter: 0.5 mm) as the counter electrode. Cyclic voltammograms (CVs) were measured using an electrochemical workstation (CHI 760E, Shanghai CH Instrument Company, China). The SAW resonators were treated by potential scanning between − 0.4 and 1 V at 50 mV $s^{-1}$ for 10 cycles in the mixed solutions (Fig. S2). After deposition, the SAW resonators were flushed using ultra-pure water and dried at ambient temperature. The Ni-$TiO_2$-Ply sensing layer was deposited on the entire surfaces of the IDTs and quartz substrate.

## Adsorption of DA on SAW sensor

DA molecules were electro-adsorbed on the Ni-$TiO_2$-Ply sensing layer of the SAW biosensor using an electric field-assisted liquid-phase oxidation method. The analyte adsorption system comprised a three-electrode system with a SAW sensor, a saturated calomel electrode (SCE), a DA electrolyte, a Pt wire electrode, and an electrochemical workstation. Electroadsorption of the DA molecules on the SAW sensor was achieved in the DA solution by cyclic voltammetry, while the potential was scanned from − 0.6 to 0.8 V at a scan rate of 20 mV $s^{-1}$ for two cycles (Fig. S3a). For human serums, the method and parameters of electroadsorption are consistent with the above content. The DA-adsorbed SAW biosensor was rinsed with ultrapure water and then dried at room temperature for 5 min.

## SAW measurement

The performances of the SAW devices were characterized using a Keysight ENA-E5071C vector network analyzer (USA) with a resolution of 625 Hz, as shown in Fig. 1a. We chose the center frequency signal ($f_0$) as the main detection signal, and the phase signal was used to assist in the analysis of the frequency shift phenomenon. The measurement range of the center frequency was 420–448 MHz, and the corresponding phase signals were collected synchronously. The

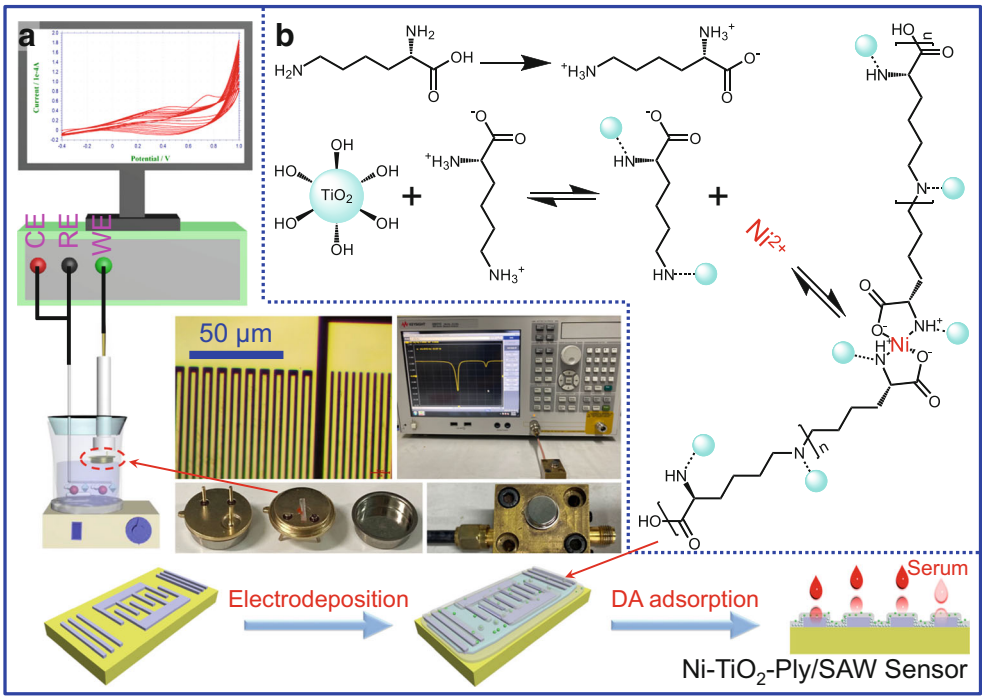


**Fig. 1** Schematics of the **a** preparation process and **b** formation mechanism of the Ni-$TiO_2$-Ply/SAW biosensor

SAW sensor was inserted into the shielding test box through the pins (Fig. 1a). The center frequency signal was then recorded, and the frequency shift, $\Delta f = f_x - f_0$, was calculated, where $f_x$ is the center frequency of the sensor for *x*-nM DA.

The SAW sensor used in the study is immersed in PBS solution, and the CVs are continuously scanned for two cycles at 20 mV $s^{-1}$ in the potential range of − 0.6 to 0.8 V to remove the adsorbed DA (Fig. S3b). The DA redox process is reversible. When the CV curve is scanned backward in the blank solution (PBS), the reaction product will be reduced to DA and re-dissolved into the PBS, thereby desorbing from the sensor. As a result, the center frequency of the SAW sensor returns to the original center frequency (Fig. S3c). Subsequently, the regenerated SAW sensor immersed in the next sample solution to electrically adsorb the DA, and the center frequency recording is continued.

## Results and discussion

### Formation mechanism of Ni-$TiO_2$-Ply layer

Figure 1 illustrates the deposition process and formation mechanism of the Ni-$TiO_2$-Ply sensing layer on the SAW device. The anatase $TiO_2$ NPs had large polarities and many unsaturated bonds on the surfaces, so the adsorbed water was polarized and converted into hydroxyl groups ($TiO_2(–OH)_n$). L-lysine has a typical zwitterionic molecular structure ($(NH_3^+)(CH_2)_4CH(NH_3^+)COO^-$). Prior to applying the electric field, a neutralization reaction occurs in the electrolyte between the $NH_3^+$– of L-lysine and the OH– on the surface of $TiO_2$ NPs. In the electrodeposition process, the $Ni^{2+}$ ions are reduced to Ni atoms and combined with the N and O atoms of L-lysine (or L-lysine combined with $TiO_2$ NPs) to form coordination compounds. Simultaneously, L-lysine (or L-lysine combined with $TiO_2$ NPs) is electropolymerized to form Ply to construct a Ni-$TiO_2$-Ply sensing layer on SAW surface. The main chemical reactions are shown in Fig. 1b.

Fig. S2 shows the CVs of Ply and Ni-$TiO_2$-Ply electrodeposited on SAW devices. Oxidative polymerization of L-lysine occurs in the range of 0.3 to 0.6 V. The reduction potential of $Ni^{2+}$ ions was around − 0.2 V, and the presence of $TiO_2$ NPs catalyzed the electropolymerization of L-lysine, so the oxidation potential was obviously shifted toward negative potentials. This experimental phenomenon further confirms the Ni-$TiO_2$-Ply layer formation mechanism suggested by Fig. 1b.

### Characterization of Ni-$TiO_2$-Ply/SAW sensor

Figures 2a and S4 show the atomic force microscopy (AFM; Agilent 5600LS, USA) topographic images of local areas of the bare, Ply, Ni-Ply, $TiO_2$-Ply, and Ni-$TiO_2$-Ply/SAW devices. After modifying the Ni-$TiO_2$-Ply sensing layer on the SAW device, the width, peak-to-valley height, and roughness of the IDT fingers obviously changed. As is seen from the line profiles of the SAW devices in Fig. S5, the width of the IDT fingers significantly increased in the Ni-$TiO_2$-Ply/SAW case, reaching 2.7 μm, while that in the bare SAW case was only 2.1 μm. Figure 2b shows that the peak-to-valley height difference of the Ni-$TiO_2$-Ply/SAW sensor (0.1267 μm) is larger than those of the bare SAW (0.1212 μm) and the other sensors. The change in the height difference is small, which indicates that the sensing material was deposited on the IDT and quartz surface at almost the same rate. Figure 2c shows the RMS roughness values of the IDT fingers of the SAW, Ply/SAW, Ni-Ply/SAW, $TiO_2$-Ply/SAW, and Ni-$TiO_2$-Ply/SAW devices. Among these, the Ni-$TiO_2$-Ply/SAW has a significantly high roughness value of 0.982, which is approximately 1.3 times that of the SAW device (0.763). However, the RMS values of the IDT fingers of the other SAW devices are lower than that of the bare SAW. The Ni and $TiO_2$ NPs are close in size to or even smaller than the Al grains. These sensitive materials are individually distributed or dispersed within the Ply polymer matrix, filling the gaps between the Al crystal grains and reducing the roughness of the IDT fingers.

Figure 2d shows the SEM image and corresponding energy-dispersive spectroscopy (EDS) elemental mapping of the Ni-$TiO_2$-Ply/SAW sensor. The signals of the Al and Si atoms were derived from the IDT of the SAW resonator. The O signal was attributed to the quartz ($SiO_2$) substrate and $TiO_2$ NPs. The Ti atoms were distributed on the quartz surface more than those on the surfaces of the Al fingers, which indicate the distribution of $TiO_2$ NPs. The C and N atoms belonging to Ply as well as the Ni atoms were distributed over the entire surface of the SAW device. The distributions of these elements indicate that Ni-$TiO_2$-Ply covered the entire area of the SAW device, but more $TiO_2$ NPs were deposited on the quartz substrate surface.

The dimensional changes of the IDT fingers and the elemental distribution of sensitive components confirmed that the Ni-$TiO_2$-Ply sensing material was successfully deposited over the entire propagation region of the SAW.

### Ni-$TiO_2$-Ply/SAW sensor assembly process

The frequency response characteristics were recorded using an E5070B network analyzer. Figures 3a and S6 show the $S_{11}$ frequency responses of the bare SAW (433.956 MHz), Ply/SAW, Ni/SAW, $TiO_2$/SAW, Ni-Ply/SAW, $TiO_2$-Ply/SAW, and Ni-$TiO_2$-Ply/SAW (433.919 MHz) devices at room temperature. The SAW devices modified with various sensing components exhibit center frequencies less than that of the bare SAW. The center frequency of the Ni-$TiO_2$-Ply/SAW is about 37 kHz lower than that of the bare SAW

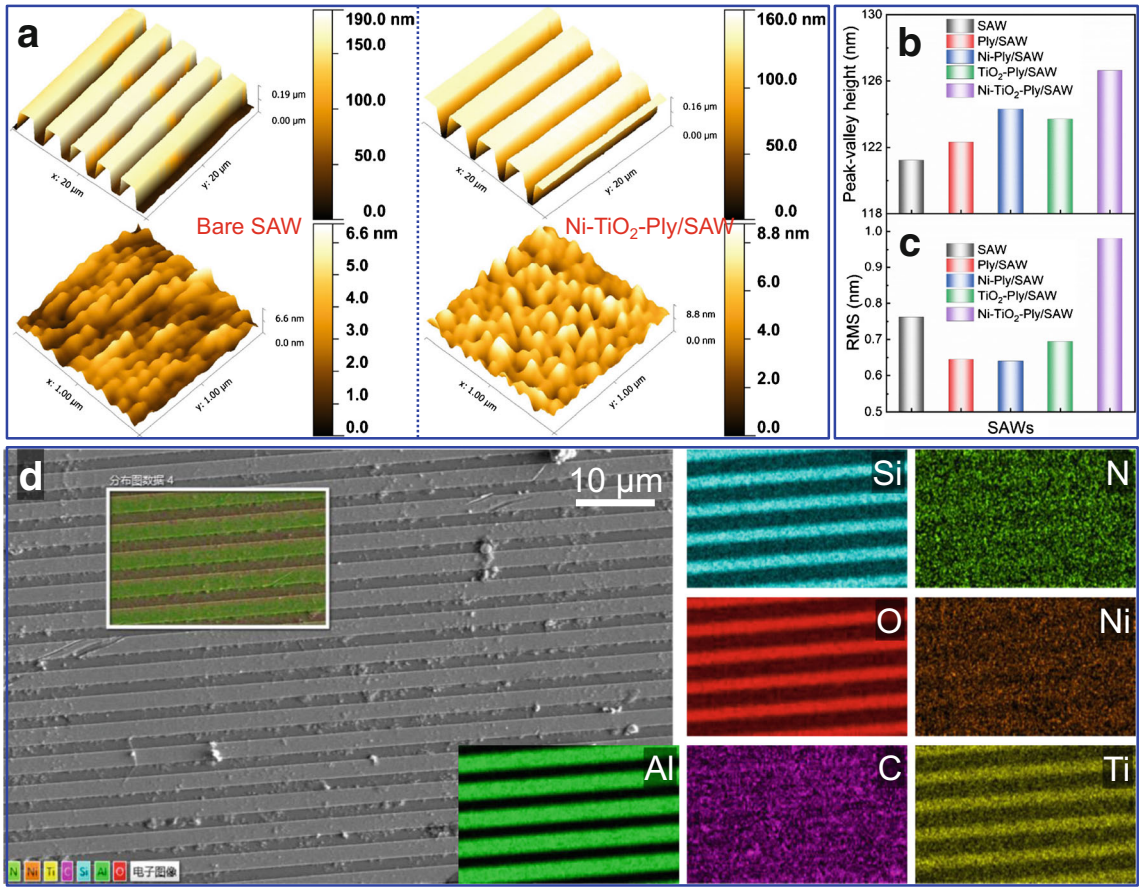


**Fig. 2** **a** AFM images of bare SAW and Ni-$TiO_2$-Ply/SAW biosensors. **b** Peak-to-valley heights of various devices. **c** RMS surface roughnesses of IDT fingers. **d** SEM image and EDS element mapping of Ni/$TiO_2$/Ply-SAW biosensor (Al, Si, O, C, Ni, N, and Ti)

resonator. In addition, the Ply and $TiO_2$ NPs significantly increase the propagation losses, but Ni reduces the propagation loss ($S_{11}$). Figure 3b shows the center frequency-phase angle curves of the SAW devices. Ply has a considerable influence on the phase angle owing to the absorption of energy along the propagation path. The $TiO_2$ NPs were more dispersed in the gaps between the IDT fingers (Fig. 2d), leading to loss of phase angle by wave scattering. The Ni NPs reduced the acoustic impedance and adjusted the energy propagation path. It can be seen that Ni NPs make up for the unfavorable effects of Ply and $TiO_2$ NPs in reducing signal resolution. To obtain a basis for optimizing the sensitive layer, we also investigated the role of three sensitive components in the DA response.

As shown in Figs. 3c and S6, the bare SAW resonator responds to the DA load but with $\Delta f$ values that are the same at different concentrations of DA. This indicates that the bare SAW resonator is sensitive to the mass load but does not selectively respond to DA. The $\Delta f$ of the Ply/SAW sensor increases with the DA concentration, indicating that Ply layer

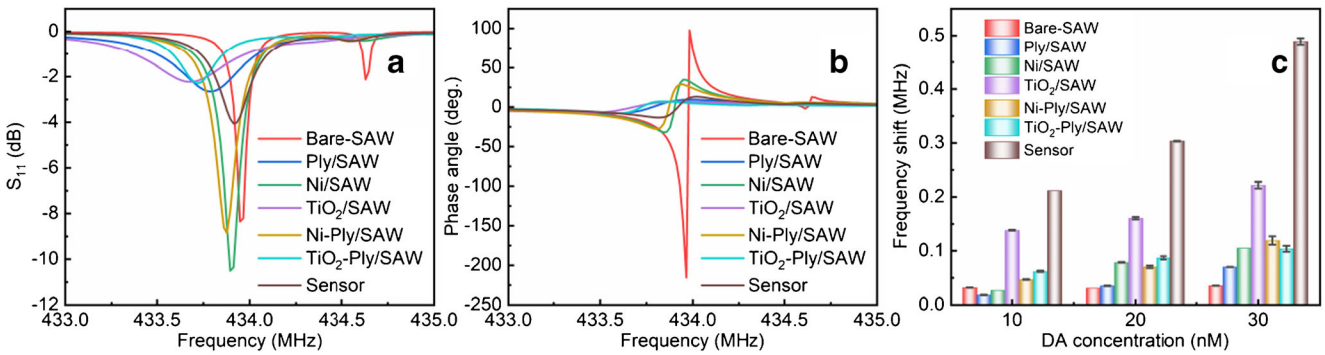


**Fig. 3** Frequency characteristics of bare-, Ply-, Ni-, $TiO_2$-, Ni-Ply-, $TiO_2$-Ply-, and Ni-$TiO_2$-Ply/SAWs of **a** loss vs. frequency and **b** phase angle vs. frequency. **c** Corresponding frequency shifts in response to DA

has DA recognition capability. Obviously, the Ni and $TiO_2$ NPs also quantitatively respond to DA. Furthermore, although the $\Delta f$ of the $TiO_2$-Ply/SAW sensor is much smaller than that of the $TiO_2$/SAW device, the changes in $\Delta f$ with DA concentration are similar. This indicates that Ply can reduce the background signal. The surface area of the $TiO_2$ NPs layer is reduced as a result of adhesion by the Ply, but the combination with the SAW device is enhanced.

Although Ply responds to DA and enhances the bonding of the sensing material on the SAW surface, it also has the negative effect of generating large propagation loss. Accordingly, the DA response signal was used as a basis for optimizing the concentration of L-lysine and the pH of the electrodeposition solution, and a condition for obtaining the best DA response was selected at 1 mM L-lysine and pH 5.0. Related data and discussions are provided in the supporting information (S3.1, Figs. S7–S9). Our analysis of the effect of frequency on temperature also confirmed that the frequency signal of the sensor in responding to DA is not affected by the ambient temperature (Fig. S10).

## Principle of DA determination

We developed a new analyte immobilization technique called electric field-assisted liquid-phase oxidation to immobilize the biomarker DA on the Ni-$TiO_2$-Ply/SAW sensor. Fig. S3a shows the CV curve recorded in the DA solution using the SAW sensor. The CV curve shows a pair of redox peaks belonging to DA/dopamine quinone (DAQ), which indicates that the sensor successfully adsorbed DA [30] according to the following reaction:

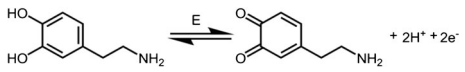


(1)

The quantity of DA electroadsorbed by the SAW sensor increases with the DA concentration as a result of the increase in the number of oxidized DA molecules. A CV method for the electropolymerization of DA onto various electrodes has been reported in the literature [30–32]. In fact, the method follows the basic principles of electrochemical quantitative analysis. The DA/DAQ redox process is also a reversible reaction: the electrochemical oxidation reaction of DA can adsorb it onto the sensor, whereas the reduction reaction desorbs DA, enabling the regeneration of the sensor for repeated use.

From a chemical point of view, the interactions of O-containing groups of the $TiO_2$ NPs with the –OH or amino groups (–$NH_2$/or –$NH_3^+$) of DA molecules were used to adsorb large amounts of DA molecules onto the sensor surface

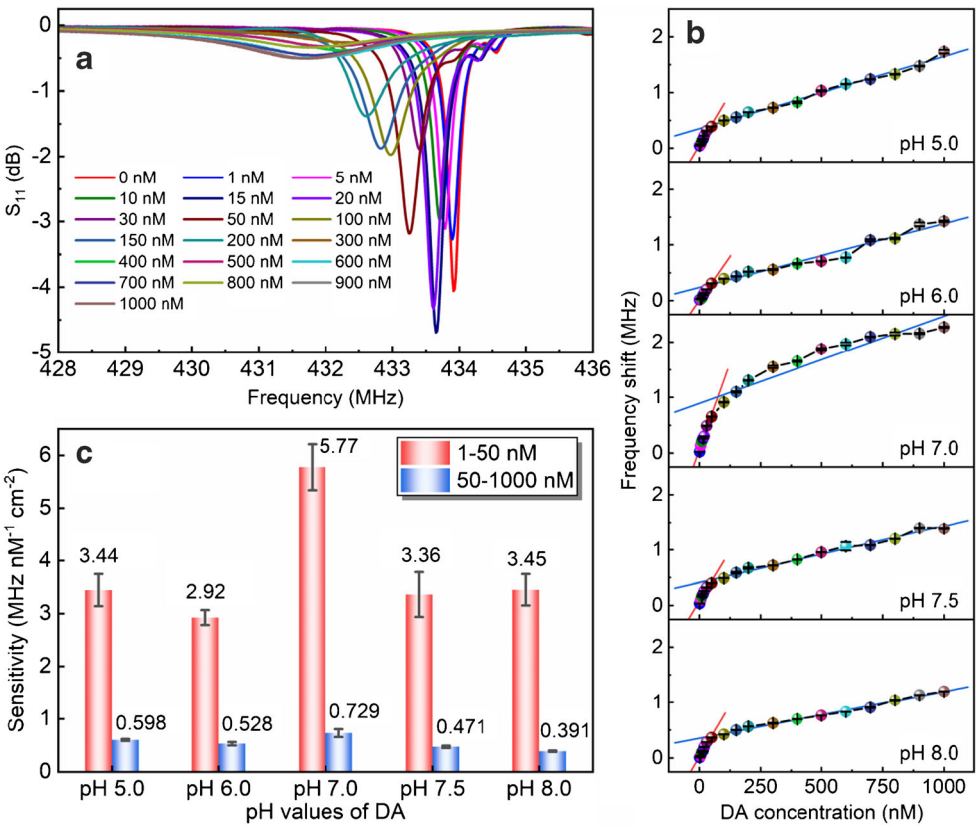


**Fig. 4** Response characteristics of the Ni-$TiO_2$-Ply/SAW sensors to different concentrations of DA. **a** Frequency characteristic curves of the Ni-$TiO_2$-Ply/SAW sensor. **b** Frequency shifts of Ni-$TiO_2$-Ply/SAW sensor for DA responses at various pH values and **c** corresponding sensitivity histograms

[33]. Furthermore, the $TiO_2$ and Ni NPs act as electrocatalysts to catalyze the carboxylation of DA (–OH → –OOH), and the carboxylated DA has a strong attraction with the $–NH_2$ of Ply. Finally, the Ni NPs contribute to the rapid capture and transfer of electrons to the sensor, promoting the oxidative self-polymerization of DA on the Ni-$TiO_2$-Ply/SAW sensor.

From a physical point of view, the frequency shift ($\Delta f$) is related to the change in SAW velocity ($\Delta v$) as follows:

$$\frac{\Delta f}{f_0} = \frac{\Delta v}{v_0} = -c_m f_0 \Delta\left(\frac{m}{A}\right) - \frac{K^2}{2}\Delta\left[\frac{1}{1+\left(\frac{v_0 c_s}{\sigma_s}\right)^2}\right] + 4c_e\frac{f_0}{v_0^2}\Delta\left(hG'\right) \quad (2)$$

where $v$ is the SAW velocity, $c_m$ is the coefficient of mass sensitivity, $m/A$ is the mass per unit area, $K^2$ is the electromechanical coupling coefficient of the piezoelectric substrate, $\sigma_s$ is the sheet conductivity of the sensing film, $c_s$ is the surface capacitance per unit length, $c_e$ is the elasticity sensitivity coefficient of the substrate, $h$ is the sensing layer thickness, and $G'$ is the real part of the shear modulus. The SAW velocity $v$ is very sensitive to the surface perturbations along the propagation path. The adsorption of DA causes changes in the mass load, conductivity, and viscoelasticity of the sensitive layer, which in turn change $\Delta f$.

In short, the process described above is a new biomarker adsorption strategy for SAW biosensors. The method is advantageous in terms of adsorbing biomarkers because it does not require complicated microfluidic channels, which allows for a simplified overall SAW sensor structure, and the sensor response can be directly measured using resonators or filters. On the other hand, there are drawbacks in that the SAW sensor cannot directly determine the liquid phase and, therefore, the frequency characteristic curve must be collected in a dry state. To further develop the approach, the constant potential adsorption/desorption method of DA should be systematically investigated, as the results could be used to rapidly develop a wireless sensor node (Videos S1 and S2).

## Quantitative analysis of DA

Figures 4a, S11, and S12 show the frequency characteristic curves of the Ni-$TiO_2$-Ply/SAW sensor in response to DA with different pH values (pH 5–8). For all pH values, the center frequencies of the sensor decrease as the DA concentration increases from 1 to 1000 nM. Figure 4b shows the working curves; the corresponding linear range, linear regression equation, sensitivity, and limit of detection (LOD) are listed in Table S1. Due to the small size of the sensor, there is a big difference in the binding strength of the single-layer and multi-

**Table 1** Comparison of Ni-$TiO_2$-Ply/SAW sensor with other methods for DA determination

| Method | Probe | Linear concentration range (nM) | LOD (nM) | DA in serum (nM) | Recovery /RSD (%) | Ref. |
|---|---|---|---|---|---|---|
| Electrochemiluminescence | Gr-CdTE QDs/TAEA-Ru | 0.001–1 | 0.0029 | 0.43 ± 0.03; 0.51 ± 0.04 | 95–108 | [6] |
| Electrochemistry | CoTSPc/Gr | 20–220 | 0.87 | – | – | [8] |
| SAW-Kalrez flow cell | CoPc-Au | – | 0.1 | – | – | [15] |
| SAW-MIP | Polypyrrole-Au | – | 10 | – | – | [25] |
| Electrochemistry | Mo NPs @/-MWCNTs | 10–1.609 × $10^6$ | 1.26 | 0 | 99.6 ± 3.21–101.4 ± 3.32 | [34] |
| Electrochemistry | $RuS_2$ NPs | 100–1 × $10^4$; 1 × $10^4$–8 × $10^4$ | 73.8 | – | – | [35] |
| Fluorescence | ZnO-CDs | 180–1.5 × $10^4$ | 1.06 | – | 105.6 ± 1.57–106.8 ± 1.9 | [36] |
| Fluorescence | CDs | 1 × $10^3$–1 × $10^4$ | 220 | – | 99.4 ± 1.0–101.8 ± 1.6 | [37] |
| Fluorescence | Trypsin Au NCs | 1 × $10^3$–1 × $10^5$ | 0.41 | – | 98.58–99.93 | [38] |
| Electrochemiluminescence | PATP@AuNPs | 1 × $10^{-6}$–1 × $10^3$ | 2 × $10^{-6}$ | 0 | 93.25 ± 2.56–112.97 ± 2.23 | [39] |
| High-performance liquid chromatographic (HPLC) | With chemiluminescence | 32.64–652.83; 652.83–6528 | 5.223 | 320.5–334.2 | 97.0 ± 2.2–101.2 ± 3.2 | [40] |
| Liquid chromatography-mass spectrometry (LC-MS) | HybridSPE-precipitation cartridge | 65–3.268 × $10^3$ | 23.5 | 36.55–226.93 | 64.97 ± 9.31–101.77 ± 6.51 | [41] |
| SAW- | Ni-$TiO_2$-Ply | 1–50; 50 × 1000 | 0.067 | 6.65–12.18 | 95.9 ± 1.54–98.89 ± 6.31 | This work |

* *CDs* carbon nanodots, *MWCNTs* multiwalled carbon nanotubes, *CoTSPc* cobalt tetrasulfonated phthalocyanine, *Gr* graphene; and *CoPc* cobalt phthalocyanine nanopillars

layer adsorption of DA on the sensor surface, which leads to two linear ranges of 1 to 50 nM and 50 to 1000 nM. For DA solutions of pH 5–8, the sensitivity of the sensor is changed, and the maximum sensitivity is 5.77 MHz $nM^{-1}$ $cm^{-2}$ at pH 7.0 (Fig. 4c). The LOD value ($S/N = 3$) of the sensor reached 0.067 nM at pH 7.0. The method for calculating LOD is described in the supporting material (S3.2). Several types of chemical sensors have been proposed for DA determination, as summarized in Table 1. Analytical methods for the measurement of DA using ECL, electrochemical, fluorescence, LC-MS, HPLC, and SAW sensors have been reported in the literature [6, 8, 34–41]. From the statistical results in Table 1, the linear concentration range of as-prepared Ni-$TiO_2$-Ply/SAW sensor tends to the middle level of various analytical methods, but the LODs are lower than those obtained using most methods. The proposed SAW sensor uses electrosorption of the analyte, a simpler and easier approach than SAW sensing using a fluid channel and a peristaltic pump [15]. Furthermore, the LOD of the SAW sensor is significantly superior to those of SAW sensors applying MIP technology [25].

## Long-term stability, selectivity, and reversibility

Figure 5a shows the relationship between the DA concentration and the frequency shift ($\Delta f$) of the sensor in pH 7.0 DA solutions with different concentrations; the corresponding frequency characteristic curves are shown in Fig. S13. Comparing the $\Delta f$ values of the DA response of the same sensor after the first and fifteenth days, the sensitivities were noted to have changed by approximately 1.6% (1–50 nM) and 5.8% (50–1000 nM).

Interfering substances of 10-nM AA, glucose, glutamate, Trp, Try, and UA were used to investigate the specificity of the sensor. The frequency response curves of the sensor were recorded in 100-nM DA and in mixtures of individual interferents and 100-nM DA (Fig. S14). The frequency response of the sensor to the DA alone was similar to that to the DA and interferent mixtures, with the latter having frequency fluctuations of less than 5% (Fig. 5b). These results indicate the favorable anti-interference ability of the proposed Ni-$TiO_2$-Ply/SAW sensor.

Reversibility was investigated by comparing the center frequency of the sensor before and after the 10-nM DA detection (Fig. S3). The sensor was regenerated in PBS using a CV method (two cycles). Following DA detection, the center frequency changed by 0.02 MHz, which is less than 10% of the $\Delta f$ in the DA response and indicates that the sensor has good reversibility characteristics in scanning the CV curve in PBS.

## Analysis of real samples

To assess the reliability of the Ni-$TiO_2$-Ply/SAW sensor in practical applications, a recovery experiment was carried out on the No. 1 serum sample, and the DA levels in five serum

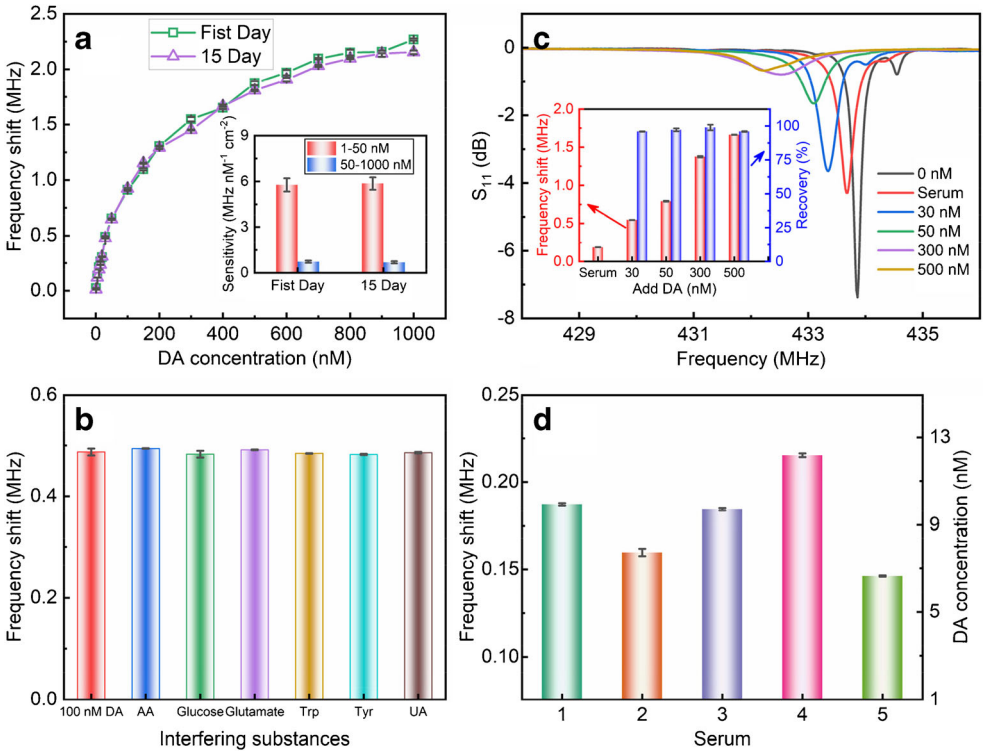


**Fig. 5** **a** Frequency shifts of the Ni-$TiO_2$-Ply/SAW sensor responding to DA on the first day and after 15 days. The inset shows the sensitivities. **b** Frequency shifts of the sensor for 100-nM DA samples containing 10-nM glucose, glutamate, Trp, Tyr, and UA, respectively. **c** Frequency characteristic curves of sensor response to DA in serum and mixtures of serum and DA reagent. The inset shows frequency shifts and recoveries. **d** Frequency shifts and DA concentrations of five serum samples

samples were determined. Figs. S15 and S16 show the corresponding frequency characteristic curves. For serum sample No. 1, 30–500-nM DA standard reagent solutions were added to the undiluted serum, and the DA recoveries were analyzed (Fig. 5c and Table S2). The DA recoveries were all in the range of 95.9 ± 1.54 to 98.89 ± 1.54%, which indicates that the detection results of the sensor were accurate. The DA concentrations in the five serum samples ranged from 6.65 to 12.18 nM. A review of the DA concentrations in human serum in the literature revealed concentrations of 0.43 ± 0.03 and 0.51 ± 0.04 nM obtained using ECL [6], 0.92–2.59 nM using fluorescence [7], 320.5($4.91 \times 10^{-8}$)–334.2 ($5.12 \times 10^{-8}$ g $mL^{-1}$) nM using HPLC [40], and 36.55–226.93 nM using LC-MS/MS [41].

## Conclusions

In this study, a Ni-$TiO_2$-Ply-modified SAW biosensor for determining DA levels in serum was investigated in detail. The main contributions are as follows. First, a Ni-$TiO_2$-Ply hybrid sensing layer was electrodeposited in situ on the finished SAW device, producing a novel SAW biosensor with the sensing layer covering the entire excitation area. Second, an electric field-assisted liquid-phase oxidation strategy was developed to selectively immobilize DA onto the SAW surface. An electric field was applied to the liquid sample to attach the analyte to the sensor, thereby producing a linear dependence between the analyte concentration and center frequency shift of the SAW device, providing a new strategy for SAW biosensor development. The electroadsorption technology can be used in conjunction with a selective sensitive membrane to selectively adsorb glucose, amino acids, and other electrochemically active species in serum. Third, we determined that the Ni-$TiO_2$-Ply/SAW biosensor has a wide concentration range and a low LOD for DA response and has the ability to determine DA in serum. If the 433-MHz biosensor can be made compatible with wireless communication modules, it can be used to track and monitor the mental states of people in battlefields and in the wilderness.

**Supplementary Information** The online version contains supplementary material available at https://doi.org/10.1007/s00604-020-04635-7.

**Funding** This study was financially supported by the National Key Research and Development Program of China (No. 2016YFB0402700) and the Natural Science Foundation of Tianjin City (Nos. 17JCZDJC32600 and 17JCQNJC00900).

### Compliance with ethical standards

**Conflict of interest** The authors declare that they have no competing interests.

## References

1. Apostolou T, Moschopoulou G, Kolotourou E, Kintzios S (2017) Assessment of in vitro dopamine-neuroblastoma cell interactions with a bioelectric biosensor: perspective for a novel in vitro functional assay for dopamine agonist/antagonist activity. Talanta 170: 69–73. https://doi.org/10.1016/j.talanta.2017.03.098
2. Taylor IM, Robbins EM, Catt KA, Cody PA, Happe CL, Cui XT (2017) Enhanced dopamine detection sensitivity by PEDOT/graphene oxide coating on in vivo carbon fiber electrodes. Biosens Bioelectron 89(Part 1):400–410. https://doi.org/10.1016/j.bios.2016.05.084
3. Vilian ATE, An S, Choe SR, Kwak CH, Huh YS, Lee J, Han Y-K (2016) Fabrication of 3D honeycomb-like porous polyurethane-functionalized reduced graphene oxide for detection of dopamine. Biosens Bioelectron 86:122–128. https://doi.org/10.1016/j.bios.2016.06.022
4. Zhao L, Li H, Gao S, Li M, Xu S, Li C, Guo W, Qu C, Yang B (2015) MgO nanobelt-modified graphene-tantalum wire electrode for the simultaneous determination of ascorbic acid, dopamine and uric acid. Electrochim Acta 168(0):191–198. https://doi.org/10.1016/j.electacta.2015.03.215
5. Diaz-Diestra D, Thapa B, Beltran-Huarac J, Weiner BR, Morell G (2017) L-cysteine capped ZnS:Mn quantum dots for room-temperature detection of dopamine with high sensitivity and selectivity. Biosens Bioelectron 87:693–700. https://doi.org/10.1016/j.bios.2016.09.022
6. Fu X, Tan X, Yuan R, Chen S (2017) A dual-potential electrochemiluminescence ratiometric sensor for sensitive detection of dopamine based on graphene-CdTe quantum dots and self-enhanced Ru(II) complex. Biosens Bioelectron 90:61–68. https://doi.org/10.1016/j.bios.2016.11.025
7. Xu Y, Wang J, Lu Y, Dai X, Yan Y (2019) Preparation of functionalized double ratio fluorescent imprinted sensors for visual determination and recognition of dopamine in human serum. Spectrochim Acta A 219:225–231. https://doi.org/10.1016/j.saa.2019.04.035
8. Diab N, Morales DM, Andronescu C, Masoud M, Schuhmann W (2019) A sensitive and selective graphene/cobalt tetrasulfonated phthalocyanine sensor for detection of dopamine. Sensors Actuators B Chem 285:17–23. https://doi.org/10.1016/j.snb.2019.01.022
9. Tang Y, Xu X, Han S, Cai C, Du H, Zhu H, Zu X, Fu Y (2020) ZnO-$Al_2O_3$ nanocomposite as a sensitive layer for high performance surface acoustic wave $H_2S$ gas sensor with enhanced elastic loading effect. Sensors Actuators B Chem 304:127395. https://doi.org/10.1016/j.snb.2019.127395
10. Mujahid A, Afzal A, Dickert FL (2019) An overview of high frequency acoustic sensors-QCMs, SAWs and FBARs-chemical and biochemical applications. Sensors 19(20):4395. https://doi.org/10.3390/s19204395
11. Oliveira GCM, Carvalho JHS, Brazaca LC, Vieira NCS, Janegitz BC (2020) Flexible platinum electrodes as electrochemical sensor and immunosensor for Parkinson's disease biomarkers. Biosens Bioelectron 152:112016. https://doi.org/10.1016/j.bios.2020.112016
12. Ji J, Pang Y, Li D, Wang X, Xu Y, Mu X (2020) Single-layered graphene/Au-nanoparticles-based love wave biosensor for highly sensitive and specific detection of Staphylococcus aureus gene sequences. ACS Appl Mater Interfaces 12(11):12417–12425. https://doi.org/10.1021/acsami.9b20639
13. Ji J, Yang C, Zhang F, Shang Z, Xu Y, Chen Y, Chen M, Mu X (2019) A high sensitive SH-SAW biosensor based 36° Y-X black LiTaO3 for label-free detection of Pseudomonas aeruginosa. Sensors Actuators B Chem 281:757–764. https://doi.org/10.1016/j.snb.2018.10.128

14. Xu Z, Yuan YJ (2018) Implementation of guiding layers of surface acoustic wave devices: a review. Biosens Bioelectron 99:500–512. https://doi.org/10.1016/j.bios.2017.07.060
15. Fourati N, Seydou M, Zerrouki C, Singh A, Samanta S, Maurel F, Aswav DK, Chehimi M (2014) Ultrasensitive and selective detection of dopamine using cobalt-phihalocyanine nanopillar-based surface acoustic wave sensor. ACS Appl Mater Interfaces 6(24): 22378–22386. https://doi.org/10.1021/am506403f
16. Jandas PJ, Luo J, Prabakaran K, Chen F, Fu YQ (2020) Highly stable, love-mode surface acoustic wave biosensor using Au nanoparticle-$MoS_2$-rGO nano-cluster doped polyimide nanocomposite for the selective detection of carcinoembryonic antigen. Mater Chem Phys 246:122800. https://doi.org/10.1016/j.matchemphys.2020.122800
17. Lei S, Deng C, Chen YQ, Li Y (2011) A novel serial high frequency surface acoustic wave humidity sensor. Sensors Actuators A Phys 167(2):231–236. https://doi.org/10.1016/j.sna.2011.01.020
18. Luo J, Luo P, Xie M, Du K, Zhao B, Pan F, Fan P, Zeng F, Zhang D, Zheng Z, Liang G (2013) A new type of glucose biosensor based on surface acoustic wave resonator using Mn-doped ZnO multilayer structure. Biosens Bioelectron 49:512–518. https://doi.org/10.1016/j.bios.2013.05.021
19. Wang C, Wang C, Jin D, Yu Y, Yang F, Zhang Y, Yao Q, Zhang G-J (2020) AuNP-amplified surface acoustic wave sensor for the quantification of exosomes. ACS Sens 5(2):362–369. https://doi.org/10.1021/acssensors.9b01869
20. Šetka M, Bahos FA, Matatagui D, Potoček M, Kral Z, Drbohlavová J, Gràcia I, Vallejos S (2020) Love wave sensors based on gold nanoparticle-modified polypyrrole and their properties to ammonia and ethylene. Sensors Actuators B Chem 304:127337. https://doi.org/10.1016/j.snb.2019.127337
21. Afzal A, Iqbal N, Mujahid A, Schirhagl R (2013) Advanced vapor recognition materials for selective and fast responsive surface acoustic wave sensors: a review. Anal Chim Acta 787:36–49. https://doi.org/10.1016/j.aca.2013.05.005
22. Xu S, Li C, Li H, Li M, Qu C, Yang B (2015) Carbon dioxide sensors based on a surface acoustic wave device with a graphene–nickel–l-alanine multilayer film. J Mater Chem C 3(16):3882–3890. https://doi.org/10.1039/c4tc02986k
23. Kamal Eddin FB, Wing Fen Y (2020) Recent advances in electrochemical and optical sensing of dopamine. Sensors (Basel) 20(4): 1039. https://doi.org/10.3390/s20041039
24. Taniselass S, Arshad MKM, Gopinath SCB (2019) Graphene-based electrochemical biosensors for monitoring noncommunicable disease biomarkers. Biosens Bioelectron 130: 276–292. https://doi.org/10.1016/j.bios.2019.01.047
25. Maouche N, Ktari N, Bakas I, Fourati N, Zerrouki C, Seydou M, Maurel F, Chehimi MM (2015) A surface acoustic wave sensor functionalized with a polypyrrole molecularly imprinted polymer for selective dopamine detection. J Mol Recognit 28(11):667–678. https://doi.org/10.1002/jmr.2482
26. Kim S, G-h M, Kim G, Kang U, Park H, Choi W (2017) TiO2 complexed with dopamine-derived polymers and the visible light photocatalytic activities for water pollutants. J Catal 346:92–100. https://doi.org/10.1016/j.jcat.2016.11.027
27. Farajikhah S, Innis PC, Paull B, Wallace GG, Harris AR (2019) Facile development of a fiber-based electrode for highly selective and sensitive detection of dopamine. ACS Sens 4(10):2599–2604. https://doi.org/10.1021/acssensors.9b01583
28. Khamrai M, Banerjee SL, Paul S, Ghosh AK, Sarkar P, Kundu PP (2019) A mussel mimetic, bioadhesive, antimicrobial patch based on dopamine-modified bacterial cellulose/rGO/Ag NPs: a green approach toward wound-healing applications. ACS Sustain Chem Eng 7(14): 12083–12097. https://doi.org/10.1021/acssuschemeng.9b01163
29. Liu T, Liu Y, Chen Y, Liu S, Maitz MF, Wang X, Zhang K, Wang J, Wang Y, Chen J, Huang N (2014) Immobilization of heparin/poly-l-lysine nanoparticles on dopamine-coated surface to create a heparin density gradient for selective direction of platelet and vascular cells behavior. Acta Biomater 10(5):1940–1954. https://doi.org/10.1016/j.actbio.2013.12.013
30. Wang JL, Li BC, Li ZJ, Ren KF, Jin LJ, Zhang SM, Chang H, Sun YX, Ji J (2014) Electropolymerization of dopamine for surface modification of complex-shaped cardiovascular stents. Biomaterials 35(27):7679–7689. https://doi.org/10.1016/j.biomaterials.2014.05.047
31. Cai JS, Huang JY, Ge MZ, Iocozzia J, Lin ZQ, Zhang KQ, Lai YK (2017) Immobilization of Pt nanoparticles via rapid and reusable electropolymerization of dopamine on TiO2 nanotube arrays for reversible SERS substrates and nonenzymatic glucose sensors. Small 13(19):1604240. https://doi.org/10.1002/smll.201604240
32. Loget G, Wood JB, Cho K, Halpern AR, Corn RM (2013) Electrodeposition of polydopamine thin films for DNA patterning and microarrays. Anal Chem 85(21):9991–9995. https://doi.org/10.1021/ac4022743
33. Dugandžić IM, Jovanović DJ, Mančić LT, Milošević OB, Ahrenkiel SP, Šaponjić ZV, Nedeljković JM (2013) Ultrasonic spray pyrolysis of surface modified $TiO_2$ nanoparticles with dopamine. Mater Chem Phys 143(1):233–239. https://doi.org/10.1016/j.matchemphys.2013.08.058
34. Keerthi M, Boopathy G, Chen SM, Chen TW, Lou BS (2019) A core-shell molybdenum nanoparticles entrapped f-MWCNTs hybrid nanostructured material based non-enzymatic biosensor for electrochemical detection of dopamine neurotransmitter in biological samples. Sci Rep 9(1):13075. https://doi.org/10.1038/s41598-019-48999-0
35. Deepika J, Sha R, Badhulika S (2019) A ruthenium(IV) disulfide based non-enzymatic sensor for selective and sensitive amperometric determination of dopamine. Microchim Acta 186(7):480. https://doi.org/10.1007/s00604-019-3622-3
36. Jana J, Chung JS, Hur SH (2019) ZnO-associated carbon dot-based fluorescent assay for sensitive and selective dopamine detection. Acs Omega 4(16):17031–17038. https://doi.org/10.1021/acsomega.9b02637
37. Chaiendoo K, Ittisanronnachai S, Promarak V, Ngeontae W (2019) Polydopamine-coated carbon nanodots are a highly selective turn-on fluorescent probe for dopamine. Carbon 146:728–735. https://doi.org/10.1016/j.carbon.2019.02.030
38. Ghosh S, Bhamore JR, Malek NI, Murthy ZVP, Kailasa SK (2019) Trypsin mediated one-pot reaction for the synthesis of red fluorescent gold nanoclusters: sensing of multiple analytes (carbidopa, dopamine, $Cu^{2+}$, $Co^{2+}$ and $Hg^{2+}$ ions). Spectrochim Acta A 215: 209–217. https://doi.org/10.1016/j.saa.2019.02.078
39. Gu Y, Wang J, Shi H, Pan M, Liu B, Fang G, Wang S (2019) Electrochemiluminescence sensor based on upconversion nanoparticles and oligoaniline-crosslinked gold nanoparticles imprinting recognition sites for the determination of dopamine. Biosens Bioelectron 128:129–136. https://doi.org/10.1016/j.bios.2018.12.043
40. Chen FN, Zhang YX, Zhang ZJ (2007) Simultaneous determination of epinephrine, noradrenaline and dopamine in human serum samples by high performance liquid chromatography with chemiluminescence detection. Chin J Chem 25(7):942–946. https://doi.org/10.1002/cjoc.200790183
41. Moriarty M, Lee A, O'Connell B, Lehane M, Keeley H, Furey A (2012) The application and validation of HybridSPE-precipitation cartridge technology for the rapid clean-up of serum matrices (from phospholipids) for the clinical analysis of serotonin, dopamine and melatonin. Chromatographia 75(21–22):1257–1269. https://doi.org/10.1007/s10337-012-2330-5